

Chandra OBSERVATIONS OF ABELL 2029: NO COOLING FLOW AND A STEEP ABUNDANCE GRADIENT

AARON D. LEWIS^{1,2}, JOHN T. STOCKE², DAVID A. BUOTE¹
 lewisa@uci.edu, stocke@casa.colorado.edu, buote@uci.edu

Received 2002 January 24; Accepted 2002 May 22

ABSTRACT

We have obtained high spatial resolution temperature and abundance profiles for the galaxy cluster Abell 2029 with the *Chandra* ACIS-S instrument. Our observations reveal that the spectra are well-fit by a single-phase gas in each annulus. While the temperature of the intracluster medium drops from ~ 9 keV at $3'$ ($260 h_{70}^{-1}$ kpc) to 3 keV in the central $5''$ ($5 h_{70}^{-1}$ kpc) of the cluster, there is no evidence for gas emitting at temperatures below 3 keV. The addition of a cooling flow component does not improve the fits, despite previous claims for a massive cooling flow. There is also no evidence for excess absorption above the Galactic N_H value. We also observe a steep Fe abundance gradient, such that $Z_{Fe} \gtrsim 2 Z_{\odot}$ (assuming meteoritic solar Fe abundance) in the core, consistent with significant enrichment from Fe-rich Type Ia supernovae in the cD galaxy. The Fe abundance drops to $\approx 0.5 Z_{\odot}$ at $3'$ ($260 h_{70}^{-1}$ kpc), in good agreement with previous *BeppoSAX* measurements. The high resolution image reveals neither a strong central point source, nor any filamentary structure related to a cooling flow or a merger. The absence of a strong merger signature argues against the creation of the wide-angle-tail radio source morphology in a merger event.

Subject headings: galaxies:clusters:individual (A2029) — cooling flows — intergalactic medium — X-ray:galaxies — galaxies:abundances

1. INTRODUCTION

Abell 2029 (A2029 hereafter) is a richness class II, Bautz-Morgan type I nearby cluster of galaxies at a redshift of $z = 0.0767$ (Abell et al. 1989). It has a very large cD galaxy (UGC 9752 = IC 1101) with a stellar envelope extending well beyond $600 h_{70}^{-1}$ kpc (Uson et al. 1991), and is one of the most optically regular rich clusters known (Dressler 1978). It has been well studied optically (see e.g., Dressler 1981; Johnstone et al. 1987), and can be characterized as a compact, relaxed, cD-galaxy dominated system, with no emission-line emitting galaxies within $600 h_{70}^{-1}$ kpc of its core (Dale & Uson 2000). Throughout this Letter, we assume a cosmology of $H_0 = 70 h_{70}$ km s⁻¹ Mpc⁻¹, $\Omega_{matter} = 0.3$, and $\Lambda = 0.7$, implying a luminosity distance to A2029 of $347 h_{70}^{-1}$ Mpc and a scale of 1.45 kpc arcsec⁻¹.

A2029 has been previously studied in the X-rays using various instruments: the *ROSAT* HRI (Sarazin et al. 1992), *ROSAT* PSPC and *ASCA* (Buote & Canizares 1996; Sarazin et al. 1998; White 2000), and *BeppoSAX* (Molendi & De Grandi 1999; Irwin & Bregman 2000). It is one of the brightest X-ray clusters in the sky ($F_X = 7.5 \times 10^{-11}$ ergs s⁻¹ cm⁻² in the 2-10 keV band, David et al. 1993), corresponding to $L_X(2 - 10\text{keV}) = 1.1 \times 10^{45} h_{70}^{-2}$ ergs s⁻¹. From *ASCA* spectra, Molendi & De Grandi (1999) find an intracluster medium (ICM) temperature in the central $2'$ of $T_X = 8.3 \pm 0.2$ keV declining to ~ 5 keV at a radius of $10'$ ($972 h_{70}^{-1}$ kpc).

Previous imaging and spectral studies have inferred a large cooling flow with $\dot{M} \simeq 400 - 600 M_{\odot}$ yr⁻¹ (Edge et al. 1992; Fabian 1994; Arnaud 1988; Peres et al. 1998), (but c.f., White 2000). However, evidence that it is not a

cooling flow includes no detection of H α or O II emission in the cD galaxy, and no blue stellar colors in the core (McNamara & O'Connell 1989). The cD galaxy also hosts a wide-angle-tail (WAT) radio source (PKS 1509+49 = 4C+06.53), which is highly unusual in a cooling flow system (Burns 1990). Simulations show that WATs may be the signatures of ongoing cluster mergers; these simulated systems also exhibit hot shock fronts (Loken et al. 1995; Roettiger et al. 1996).

Obviously the relaxed cooling flow and merger/hot shock scenarios are mutually exclusive, and for this reason we have obtained high spatial resolution imaging spectroscopy with the *Chandra* observatory in order to

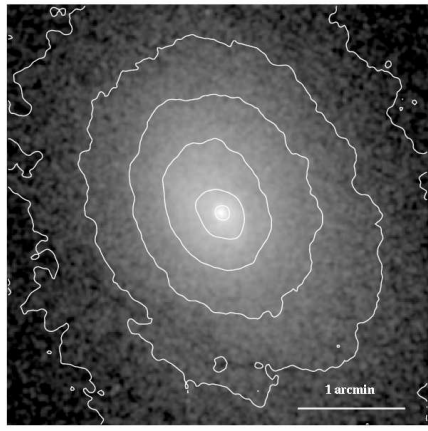


FIG. 1.— *Chandra* ACIS-S image of Abell 2029. The image is $4'$ ($348 h_{70}^{-1}$ kpc) on a side and has been smoothed with a Gaussian of $\sigma = 2''$. North is up and East is left. Logarithmically spaced contours are overlaid to indicate morphology.

¹ University of California, Irvine, Department of Physics and Astronomy, 4171 Frederick Reines Hall, Irvine, CA, 92697-4575

² Center for Astrophysics and Space Astronomy, University of Colorado, 389 UCB, Boulder, CO 80309

investigate this enigmatic object. In this Letter we describe the global temperature structure, resolved metal abundances, as well as highly spatially-resolved spectral properties of the central regions. A future publication will measure the dark matter profile.

We note that the authors of most X-ray spectral analyses to date have used “photospheric” Fe abundances. Following the suggestion of Ishimaru & Arimoto (1997), we use the abundance measurements of Anders & Grevesse (1989) for spectral fitting, except for Fe where we use the correct “meteoritic” value, $\text{Fe/H} = 3.24 \times 10^{-5}$ by number. This results in Fe abundance values a factor 1.44 times larger than the “photospheric” values. We will note this factor when comparing to other work.

2. OBSERVATIONS AND DATA REDUCTION

A2029 was observed with the *Chandra* observatory on 2000 12 April for a deadtime-corrected exposure of 19.8 ksec. The cluster was centered on the backside-illuminated S3 chip, operating at a temperature of -120 C. The data were re-processed using CIAO 2.2.1 and version 2.7 of the *Chandra* calibration database (CALDB). We mitigated the effects of charge transfer inefficiency using the ACISCTi-Corrector.1.37 software³ (Townsley et al. 2000). The data were screened for energy (0.3 to 8.0 keV), grade (ASCA 02346), and status (0). We examined the lightcurve for possible flaring of the background, and removed 365 seconds of suspect exposure. We then scaled and subtracted the available source-free extragalactic sky background maps⁴ using the make_acisbg software created by Maxim Markevitch (see, e.g. Markevitch et al. 2000).

In Figure 1 we present the smoothed, background-subtracted ACIS-S image of A2029 in the energy range 0.3 – 8.0 keV. The image reveals A2029 to be quite regular; although there are some position-angle dependent variations within a 1' radius, we find no evidence of bright shock fronts, filaments, or bright point sources. The X-ray emission is somewhat elliptical, with a position angle of $\sim 25^\circ$ (North to East), consistent with the *ROSAT* PSPC image analysis of Buote & Canizares (1996).

3. SPATIALLY RESOLVED SPECTRAL PROPERTIES

To analyze the spectrum of the hot ICM, we extracted spectra from eleven concentric annuli centered on the peak of the X-ray emission (coincident with the BCG at RA = $15^h10^m56.^s2$, Decl. = $+05^\circ44'44''$, J2000). The annuli were of varying widths providing approximately 10,000 counts per annulus in the energy range 0.3 – 8.0 keV, except that to investigate the core with maximum spatial resolution, we chose a central region 5'' in radius, containing approximately 5,000 counts.

3.1. Radial Temperature Profile

Using XSPEC, we fit the extracted spectra with the APEC plasma emission model⁵ absorbed by neutral hydrogen. We adopt the weighted average Galactic value of $\text{N}_H = 3.14 \times 10^{20} \text{ cm}^{-2}$ obtained from the W3N_H HEASARC tool. The Fe abundance was allowed to be a

free parameter, with all other elements tied to Fe in their solar ratios.

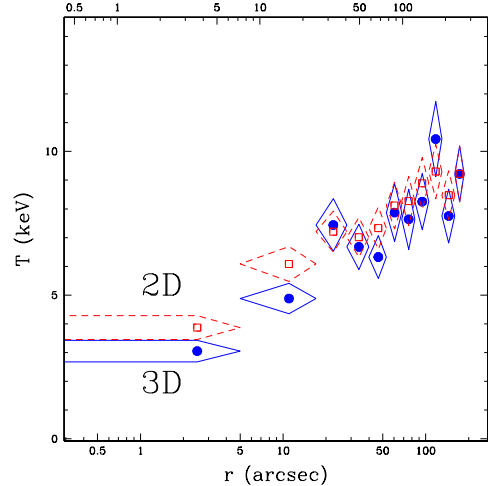


FIG. 2.— *Chandra* radial temperature profile of A2029. Solid lines (and filled circles) are the results of the 3D spectral deprojection. Dotted lines (and open squares) are the 2D analysis. Horizontal axis shows both arcsec (*lower axis*) and h_{70}^{-1} kpc (*upper axis*) units.

To properly recover the three-dimensional properties of the X-ray emitting ICM, we have performed a spectral deprojection analysis using the XDEPROJ code of Buote (2000). We start at the outside working our way to the core in an “onion-peeling” method which accounts for the cumulative projected emission from the outer annuli, obtaining temperatures, densities, abundances, and any other desired parameters. For details of our deprojection technique see Buote (2000) and Buote et al. (2002). To estimate the uncertainties on the fitted parameters we simulated spectra for each annulus using the best-fitting models and fit the simulated spectra in exactly the same manner as the actual data. From 100 Monte Carlo simulations we compute the standard deviation for each free parameter which we quote as the “1 σ ” error. The reference model we have used is APEC with deprojection, denoted APEC (3D). For comparison, we have also performed a standard two-dimensional analysis with no deprojection, denoted APEC (2D).

In Figure 2 we show the radial temperature profile of A2029 derived from the 3D analysis (*solid lines* and filled circles) and the 2D analysis (*dotted lines* and open squares). Figure 2 shows an obvious drop in temperature in the core, with increasing values at larger radii (our final bin is between 160-186 arcsec, 2.7 – 3.1', or 232-270 h_{70}^{-1} kpc). The 3D model shows a more dramatic drop in the center, the signal of which is masked in the 2D fits as hotter gas from larger radii is observed in projection over the cooler core. We observe the gas temperature to be approximately 8-10 keV at 100-200 arcseconds. The gas drops to a minimum temperature of 3.1 ± 0.4 keV in the inner 5''. The data suggest a continuing increase in temperature, though the profile is possibly flattening at the limit of our measurements. We note that the sharp bin-to-bin fluctuations seen for the 3D model in the four outermost annuli are due to the nature of the 3D deproj-

³ Available from the *Chandra* contributed software page at <http://asc.harvard.edu/cont-soft/soft-exchange.html>

⁴ The background maps have been CTI-corrected in exactly the same manner as the source data.

⁵ We have also performed fits with the MEKAL model. We find no statistical differences in temperature or abundance measurements.

jection algorithm, and should not be considered a physical feature. This effect can be avoided by regularizing (in effect smoothing) the parameters, which we do not perform for this Letter (but see Buote 2000 for details of the procedure). The 3D fluctuations in the outer bins vary about the 2D temperature values in these bins without significant bias. This is expected because at large radii the gas is nearly isothermal and also suffers the least from projection effects, such that the 2D profile can be used to verify the 3D results in these annuli. The quality of the fits is only marginally improved using the 3D vs. 2D method, with the most improvement occurring in the inner 2 annuli where we also observe the largest change in temperature.

The formal quality of the spectral fits is quite good ($\chi^2/\text{dof} = 134.02/111$ in the central annulus, for the reference model), but there exist significant (10-15%) residuals below 0.5 keV, where the data are in excess of the model. At these energies we have either under-subtracted the background or there are calibration issues outstanding. In the outer annuli where the observations are background dominated (especially at high energy), the background estimate seems secure and we are inclined to doubt the calibration at $E < 0.5$ keV. Between 0.65 and 0.75 keV, the data fall below the model in the inner three annuli, but this ‘absorption feature’ is much sharper than the spectral resolution of the S3 chip and its nature is not clear. These features can be seen in Fig. 3, wherein we present the spectrum and residuals from the fit in Annulus 2 (between 5 and 17'').

Allowing the neutral hydrogen column density to be a free parameter in the fits results in N_H values less than half the Galactic value in the outer regions which climb to slightly higher than Galactic in the central bin. As a test, we have performed an additional set of fits eliminating all energies below 0.7 keV (APEC (3D-0.7) $\chi^2/\text{dof} = 87.10/91$). We have repeated this exercise with all the other models presented in this Letter. We find that the removal of low energy residuals does not change either the temperature or abundance measurements beyond their errors. The rise in N_H in the center would appear to accommodate the ‘absorption feature’ near 0.6 keV in the central bin, but elimination of energies below 0.7 keV merely weakens the constraint on N_H without lowering the fitted value. In either case, there is almost no improvement in the fit quality in the inner 2 annuli. Freeing N_H does result in a significant improvement in the fit quality for annuli 3-11. As expected, eliminating energies below 0.7 keV in the fits obtains higher (but still sub-Galactic) N_H values. Although it is possible there is a decrement in actual Galactic N_H along the line of sight to A2029, this would not be consistent with any previous observations (at a variety of wavelengths).

3.2. Fe abundance profile

In Figure 4 we show the radial metal abundance profile of A2029 from the APEC (3D) model fits. Ratio of Fe to its solar (meteoritic) value is shown. We observe subsolar (approximately $0.5 Z_\odot$) abundances outside of 20'', and a very sharp increase in the core to $\sim 2 Z_\odot$. The abundances of other elements (S, Si, Mg and O) are not constrained to better than $\sim 50\%$ except in a few central bins where the

⁶ see the Chandra Proposers’ Observatory Guide Rev 3.0.

emission lines are more pronounced relative to the lower

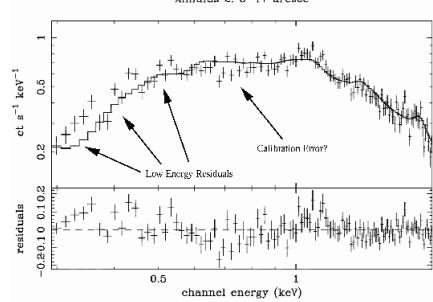


FIG. 3.— Spectrum in Annulus 2 (5-17'') between 0.3 and 2.0 keV. Fractional residuals shown at bottom. Model is APEC (3D), with Galactic N_H absorption. Note that we do not see these residual features at larger radii.

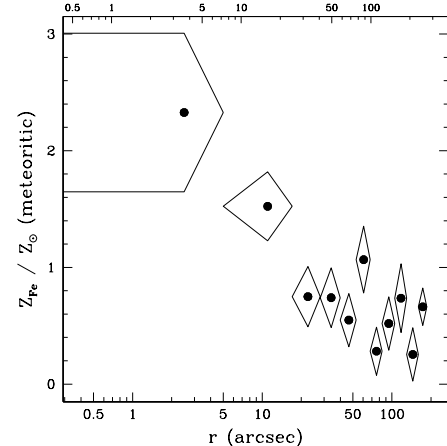


FIG. 4.— Chandra deprojected radial Fe abundance profile of A2029. Horizontal axis shows both arcsec (lower axis) and kpc (upper axis) units.

temperature ICM. As we are unable to place significant constraints on any interesting abundance ratios we do not present these data. We note that allowing additional element abundances to vary does not effect the Fe abundances beyond the errors shown in Figure 4.

Our measurements are entirely consistent with the \sim arcmin spatial resolution *BepoSAX* results of Molendi & De Grandi (1999) and Irwin & Bregman (2001), who measured $Z_{Fe} \sim 0.5 Z_\odot$ ($0.72 Z_\odot$ in meteoritic units) within the central 2', declining to ~ 0.2 (0.29) at larger radii ($\sim 10'$). An emission-weighted average of our best-fitting Chandra Fe abundance measurements in bins 1-9 ($0 - 2.2'$) yields $Z_{Fe} = 0.77 Z_\odot$ (meteoritic). We also see a decline to values consistent with $0.35 Z_\odot$ (within our errors) for our outermost data points which extend to 3'.

4. ANALYSIS OF THE CORE

The unsurpassed spatial resolution of Chandra allows us to investigate the core of A2029 with high S/N in the central 5'' region. The observation of A2029 was pointed 1.3' from the ACIS-S aimpoint (the cluster center was placed 1.2' south, and 30'' east of the aimpoint to place more extended emission on the S3 chip), which should result in an effective PSF of $\lesssim 1.5''$ FWHM (it is within the region of the detector where the encircled energy within 1'' is $\geq 50\%$ ⁶).

4.1. Alternative Spectral Models

From our single-temperature fit we obtain $T_X = 3.1 \pm 0.4$ keV, and a good fit to several strong emission features across the entire spectrum, except for the low energy absorption feature near 0.6 keV. Although the quality of the fit in this annulus is acceptable ($134.02/111 \chi^2/\text{dof}$), we have investigated additional or alternative spectral models.

We have added to the first three annuli in turn: a second temperature component (APEC+APEC (3D) $\chi^2/\text{dof} = 132.60/108$), a constant pressure cooling flow, with the material cooling from the temperature of the APEC model (APEC+CF (3D) $\chi^2/\text{dof} = 133.29/109$), and a power law model (APEC+POW (3D) $\chi^2/\text{dof} = 133.62/109$). Each model was absorbed by N_H , which was fixed to the Galactic value for all models except CF. None of these models provided a significant improvement to the fits. The cooling flow fit yields a cooling rate of $0.0 \pm 0.7 M_\odot \text{ yr}^{-1}$, similar to other recent XMM-Newton analyses (see, e.g., Kaastra et al. 2001; Böhringer et al. 2002).

4.2. Constraints on a Central Point Source

In Figure 5 we show the azimuthally averaged surface brightness profile of A2029 obtained from counts in the 0.3 – 8.0 keV band. We extracted counts from the background-subtracted image in annuli 1.5" wide out to a radius of 186". We then subtracted an in-field background taken from a region outside the extraction area still on the S3 chip (the southwest corner). For the present analysis of the core, the impact of an exposure map is negligible, and we have not performed such a correction.

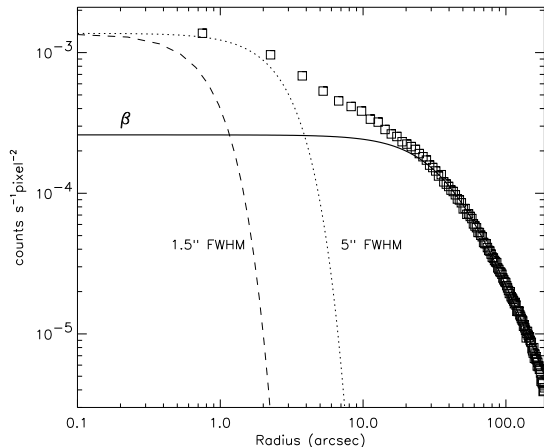


FIG. 5.— *Chandra* surface brightness profile of A2029 in the 0.3 – 8.0 keV band (open squares). Overlaid are two Gaussians of FWHM 1.5 (dashed curve) and 5" (dotted curve), respectively, as well as a β -model fit (solid curve), with $\beta = 0.60$, $r_{\text{core}} = 42''$.

The profile is smooth, and well constrained to the limit of our observations. There is a significant peak in the profile at $\lesssim 20''$. This peak is wider than a Gaussian of 5" FWHM (overlaid as a dotted line), and thus unambiguously resolved (for reference we have also overlaid a Gaussian of 1.5" FWHM [dashed line] representing an upper limit to the ACIS PSF). We also show a standard β -model fit to the data omitting the inner 20" to obtain an acceptable fit. Because we see no spectral evidence for either a power-law source, or a cooling flow, we suggest that the peak may represent a cusp in the gravitational potential due to the mass of the cD galaxy.

5. DISCUSSION

We have analyzed high spatial resolution *Chandra* spectra of the A2029 cluster of galaxies. We observe both strong temperature and abundance gradients within the central arcmin, with T_X dropping to ~ 3 keV, and Z_{Fe} rising to $\approx 2 Z_\odot$. We find no evidence for excess absorption in the core, though there are some remaining residuals in the low energy (≤ 0.7 keV) region of the spectrum which are not yet understood. Additional model components (including a cooling flow) are not required, and do not improve the fits. Thus, A2029 bears no evidence of multi-phase gas, refuting earlier claims of $\dot{M} \sim 400$ – $600 M_\odot \text{ yr}^{-1}$ and thus is similar to, although more extreme than, many other recent *Chandra* and *XMM* observations (see McNamara 2002, for a review). From the image, we find no evidence of a strong shock or major cluster merger, and thus a lack of support for the Loken et al. (1995) model for producing WAT radio sources in cluster merger events. There is a small peak in the inner 10" of the surface brightness profile, indicating a second component in excess of a standard β -model.

The super-solar Fe abundance measurements in the core of A2029 are suggestive of enrichment by metals created by Fe-rich SN Ia and ejected from the cD and other galaxies in the core. Since the gaseous system is relaxed and fairly undisturbed (no recent mergers), this gradient could have been maintained to the present epoch from an earlier time. This also agrees with the analysis of De Grandi & Molendi (2001) (although we now resolve the enrichment at $< 2'$), who found that the abundance gradient matched the stellar light profile of the galaxies in the cluster core.

This work was supported by *Chandra* grant G00-1021X. ADL thanks Beth Lewis for her ongoing support.

REFERENCES

Abell, G. O., Corwin, H. G., & Olowin, R. P. 1989, ApJS, 70, 1
 Anders, E. & Grevesse, N. 1989, Geochim. Cosmochim. Acta, 53, 197
 Arnaud, K. A. 1988, in NATO ASIC Proc. 229: Cooling Flows in Clusters and Galaxies, 31–40
 Böhringer, H., Matsushita, K., Churazov, E., Ikebe, Y., & Chen, Y. 2002, A&A, 382, 804
 Buote, D. A. 2000, ApJ, 539, 172
 Buote, D. A. & Canizares, C. R. 1996, ApJ, 457, 565
 Buote, D. A., Lewis, A. D., Brighenti, F., & Mathews, W. G. 2002, ApJ, submitted
 Burns, J. O. 1990, AJ, 99, 14
 Dale, D. A. & Uson, J. M. 2000, AJ, 120, 552
 David, L. P., Slyz, A., Jones, C., Forman, W., Vrtilek, S. D., & Arnaud, K. A. 1993, ApJ, 412, 479
 De Grandi, S. & Molendi, S. 2001, ApJ, 551, 153
 Dressler, A. 1978, ApJ, 226, 55
 —. 1981, ApJ, 243, 26
 Edge, A. C., Stewart, G. C., & Fabian, A. C. 1992, MNRAS, 258, 177
 Fabian, A. C. 1994, ARA&A, 32, 277
 Irwin, J. A. & Bregman, J. N. 2000, ApJ, 538, 543
 —. 2001, ApJ, 546, 150

Ishimaru, Y. & Arimoto, N. 1997, PASJ, 49, 1

Johnstone, R. M., Fabian, A. C., & Nulsen, P. E. J. 1987, MNRAS, 224, 75

Kaastra, J. S., Ferrigno, C., Tamura, T., Paerels, F. B. S., Peterson, J. R., & Mittaz, J. P. D. 2001, A&A, 365, L99

Lothenbach, C., Roettiger, K., Burns, J. O., & Norman, M. 1995, ApJ, 445, 80

Markevitch, M., Ponman, T. J., Nulsen, P. E. J., Bautz, M. W., Burke, D. J., David, L. P., Davis, D., Donnelly, R. H., Forman, W. R., Jones, C., Kaastra, J., Kellogg, E., Kim, D.-W., Kolodziejczak, J., Mazzotta, P., Pagliaro, A., Patel, S., Van Speybroeck, L., Vikhlinin, A., Vrtilek, J., Wise, M., & Zhao, P. 2000, ApJ, 541, 542

McNamara, B. R. 2002, in ASP Conf. Ser., X-rays at Sharp Focus: Chandra Science Symposium, ed. S. Vrtilek, E. M. Schlegel, & L. Kuhri (San Francisco: ASP), astro-ph/0202199

McNamara, B. R. & O'Connell, R. W. 1989, AJ, 98, 2018

Molendi, S. & De Grandi, S. 1999, A&A, 351, L41

Peres, C. B., Fabian, A. C., Edge, A. C., Allen, S. W., Johnstone, R. M., & White, D. A. 1998, MNRAS, 298, 416

Roettiger, K., Burns, J. O., & Loken, C. 1996, ApJ, 473, 651

Sarazin, C. L., O'Connell, R. W., & McNamara, B. R. 1992, ApJ, 389, L59

Sarazin, C. L., Wise, M. W., & Markevitch, M. L. 1998, ApJ, 498, 606

Townsley, L. K., Broos, P. S., Garmire, G. P., & Nousek, J. A. 2000, ApJ, 534, L139

Uson, J. M., Boughn, S. P., & Kuhn, J. R. 1991, ApJ, 369, 46

White, D. A. 2000, MNRAS, 312, 663